Title

The Electrical and Structural Substrate of Arrhythmogenic Right Ventricular Cardiomyopathy Determined Using Noninvasive Electrocardiographic Imaging and Late Gadolinium Magnetic Resonance Imaging

Running Title

Electrophyisologic & Structural Substrate of ARVC

Authors

Christopher M Andrews[1]* (BS), Neil T Srinivasan[2,3]* (MD), Stefania Rosmini[3] (MD), Heerajnarain Bulluck[3] (MD), Michele Orini[2,3] (PhD), Sharon Jenkins[2,3] (BSc), Antonis Pantazis[2,3] (MD), William J McKenna[2,3] (MD DSc), James C Moon[3] (MD), Pier D Lambiase[2,3]† (MD PhD), and Yoram Rudy[1,4]† (PhD)

*CMA & NTS contributed equally to this manuscript

†PDL & YR are co-senior authors

Institutional Affiliations

[1]Cardiac Bioelectricity and Arrhythmia Center and Department of Biomedical Engineering, Washington University in St. Louis, St. Louis, MO, USA

[2]Department of Cardiac Electrophysiology, The Barts Heart Center, St Bartholomew's Hospital, London, UK

[3]Institute of Cardiovascular Science, University College London, London, UK

[4]Department of Medicine, Cardiovascular Division, Washington University in St. Louis, St. Louis, MO, USA

Corresponding Author:

Yoram Rudy, PhD, Director,

Cardiac Bioelectricity and Arrhythmia Center

Washington University in St. Louis

Campus Box 1097, 290 Whitaker Hall

One Brookings Drive

St. Louis, Missouri, 63130, USA

Tel: 314-935-8160

Fax: 314-935-8168

E-mail: rudy@wustl.edu

Website: http://rudylab.wustl.edu/

Word Count: 6936

Journal Subject Terms

Electrophysiology, Sudden Cardiac Death, Imaging

Abstract

Background: Arrhythmogenic right ventricular cardiomyopathy (ARVC) is a significant cause of sudden cardiac death in the young. Improved noninvasive assessment of ARVC and better understanding of the disease substrate are important for improving patient outcomes.

Methods and Results: We studied 20 genotyped ARVC patients with a broad spectrum of disease using Electrocardiographic Imaging (ECGI; a method for noninvasive cardiac electrophysiology (EP) mapping) and advanced late gadolinium enhancement (LGE) cardiac magnetic resonance scar imaging. Compared to 20 healthy controls, ARVC patients had longer ventricular activation duration (median 52 vs 42 ms; $p = 0.007$) and prolonged mean epicardial activation-recovery intervals (a surrogate for local action potential duration; median 275 vs 241 ms; $p = 0.014$). In these patients, we observed abnormal and varied epicardial activation breakthrough locations, and regions of non-uniform conduction and fractionated electrograms. Non-uniform conduction and fractionated electrograms were present in the early concealed phase of ARVC. EP abnormalities co-localized with LGE scar, indicating a relationship with structural disease. Premature ventricular contractions (PVCs) were common in ARVC patients with variable initiation sites in both ventricles. PVC rate increased with exercise, and within anatomical segments it correlated with prolonged repolarization, electrical markers of scar, and LGE (all $p < 0.001$).

Conclusions: ECGI reveals EP substrate properties that differ in ARVC patients compared to healthy controls. A novel mechanistic finding is the presence of repolarization abnormalities in

regions where ventricular ectopy originates. The results suggest a potential role for ECGI and LGE in early diagnosis and non-invasive follow-up of ARVC patients.

Key Words:

arrhythmogenic right ventricular cardiomyopathy, electrocardiographic imaging, late gadolinium enhancement

Arrhythmogenic right ventricular cardiomyopathy (ARVC) [abbreviations are defined in **Supplemental Table S1**] is an important hereditary cause of sudden cardiac death in young individuals with an estimated prevalence as high as 1:1000 [1,2]. The ARVC phenotype is progressive, consisting of an early concealed phase, overt arrhythmias, and heart failure. However, penetrance is variable and the first manifestation of the disease may be sudden cardiac death [1,2]. Diagnosis and treatment of ARVC are challenging, with implications for family screening and risk stratification [3,4].

ARVC is characterized by fibro-fatty infiltration of the myocardium with an epicardial predominance, suggesting that the disease progresses from epicardium to endocardium [5]. Fibro-fatty replacement in ARVC results from desmosomal mutations that lead to progressive cardiomyocyte death [6]. The desmosomal mutations cause decreased function of sodium channels and gap junctions in cardiomyocytes [6,7]. Exercise hastens disease progression by elevating myocardial wall stress, especially in the right ventricle (RV) [8], and has been linked to episodes of sudden cardiac death. Human and murine studies demonstrated that electrophysiological changes precede the structural disease [9]. Though originally described as a RV disease, there is increasing evidence for non-classical presentation with both biventricular and left ventricular (LV)-dominant disease [10].

Definitive diagnosis of ARVC requires histological demonstration of fibrofatty replacement of myocardium or the presence of a known ARVC genotype. Biopsy is challenging because the fibro-fatty infiltration may be patchy and epicardial. Genotypes linked to ARVC are present in only 30-40% of cases. Current diagnosis utilizes a combination of structural, functional, and

electrophysiological (EP) criteria [3]. However, diagnosis is challenging because of the progressive nature of ARVC and its early concealed phase. The only treatment proven to prevent sudden cardiac death in ARVC patients is the implantable cardioverter defibrillator (ICD). However, ICD implantation carries risks, and primary prevention indications remain a matter of debate [4,11].

Effective non-invasive modalities and improved understanding of ARVC arrhythmia mechanisms are essential for accurate diagnosis and risk stratification. As stated in a recent editorial, access to the epicardium for electrical measurements can enhance earlier disease detection. However, direct epicardial access is challenging and limited to experienced clinical centers [12]. The present study employs a noninvasive method (Electrocardiographic Imaging: ECGI; also referred to as Electrocardiographic Mapping (ECM) or body-surface mapping) [13] for epicardial EP mapping and the latest generation of magnetic resonance imaging (MRI) for cardiac structure (cardiac MRI (CMR) with advanced late gadolinium enhancement (LGE) using motion correction reconstruction) [14]. We applied ECGI and LGE to study the electrical and structural substrates in ARVC patients. These two techniques are safe, noninvasive, and well suited to longitudinal assessment of ARVC patients. The goal of this study is to provide insight into the myocardial substrate and arrhythmia mechanisms in ARVC. It also constitutes a preliminary exploration of the suitability of combined ECGI and LGE for diagnosis and risk stratification of ARVC patients.

Methods

Patient Cohort

Twenty ARVC patients with a broad spectrum of structural and electrophysiological disease were enrolled at the Heart Hospital, UCLH, London, UK. All patients were genotyped for desmosomal mutations. Patient characteristics are summarized in **Table 1** (additional clinical characteristics provided in **Supplemental Tables S2 and S3**). The study was approved by the National Research Ethics Service Committee London (14/LO/0360) and the Human Research Protection Office at Washington University in St. Louis. All patients provided written informed consent. The study conformed to the declaration of Helsinki.

ECGI and MRI

The ECGI method was developed and validated in our laboratory and described previously [13]. A schematic of the procedure is presented in **Supplemental Figure S1**. Briefly, 256 uniformly distributed body-surface electrocardiograms (ECGs) were recorded simultaneously using a portable recording system (ActiveTwo, BioSemi, Netherlands). Patients exercised on a supine ergometer for two minutes, followed by a ramp protocol of fifteen Watts/minute to a maximum heart rate (HR) of 120 beats/minute. Recordings were performed in the supine position at rest, during exercise, and immediately following exercise cessation. ECGI data were transferred to the Rudy lab for data processing, map construction, and analysis.

Following the recording protocol, CMR was performed in a 1.5 T scanner (Magnetom Avanto, Siemens Medical Solutions, Germany). Prior to the scan, recording electrodes were replaced with MRI-visible markers so the electrode positions could be obtained in the same coordinate system as the heart geometry. A navigated anatomical sequence was used so the ECGI electrical and anatomical data could be merged. Conventional cine imaging and advanced LGE imaging

were conducted following the thorax scan. The contrast agent was 0.1mmol/Kg of Gadoterate meglumine (Dotarem, Guerbet S.A., Paris, France) with LGE images acquired 5-15 minutes post-contrast. The LGE sequence was a single shot steady state free precession phase sensitive inversion recovery sequence [14] with motion corrected averaging and high resolution (typical matrix: 144 x 256; voxel size 2.0 x 1.5 x 6.0 mm^3). Two patients declined contrast injection.

Unipolar epicardial electrograms (EGMs) were reconstructed using previously described methods [13] (additional ECGI methodology references in **Supplement**). Briefly, the heart-torso geometry obtained from the MRI was used to compute a transfer matrix relating epicardial potentials to torso potentials. The inverse problem was solved to compute epicardial EGMs from the recorded ECGs. Typically, 1000 EGMs were computed over the entire ventricular epicardium. EGMs over the valve plane were excluded from analysis. Epicardial activation and repolarization maps were constructed from the EGMs. ECGI reconstructions of sinus rhythm were computed for each patient at resting HR prior to exercise and at elevated HR immediately after exercise cessation. Additionally, the epicardial activation sequence was computed for each unique premature ventricular contraction (PVC) morphology observed.

Analysis

Segmentation

ECGI maps and LGE images for each patient's ventricles were divided into basal, mid, and apical regions. Basal and mid regions were further subdivided into anterior, anterolateral, inferolateral, and inferior regions. Apical regions were subdivided into anterior and inferior

regions. EGM measures for each region were computed as the mean value from all EGMs within the region.

CMR Analysis

CMR analysis was performed using CVI42 software (Circle Cardiovascular Imaging Inc.,Version 5.1.2[303], Calgary, Canada). For the analysis of LGE in the LV, epicardial and endocardial borders were manually drawn on the short axis slices and the anterior RV insertion point was identified. The Otsu semi-automated technique was used to quantify LGE and was displayed on a bullseye plot as relative enhanced area (percentage) per segment on the 16-segment American Heart Association model.

For the analysis of the RV LGE, a segmentation model was created using short axis images. Basal, mid and apical segments were identified using the papillary muscles as markers and divided into anterior, anterolateral, inferolateral and inferior segments for the basal and mid RV segments and as apical anterior and apical inferior segments for the RV apical segments.
The amount of RV LGE was quantified visually as 0 (no LGE), 1 (some LGE), or 2 (high LGE) independently by 2 operators with 3 years of experience in CMR each (SR and HB). The operators' RV LGE quantification differed initially in 2 segments. Following additional analysis of these segments, the reviewers reached a consensus. Analyses of the ECGI and CMR data were conducted independently with investigators blinded to the results of the other modality.

Electrogram Analysis

Reconstructed unipolar epicardial EGMs were processed to compute local electrical measures. Activation times (ATs) were computed as the time of steepest negative time-derivative of voltage ($-dV/dt_{max}$) in the local QRS complex. Recovery times (RTs) were computed as the time of steepest positive time-derivative (dV/dt_{max}) during the T-wave [15]. Activation-recovery intervals (ARIs, a surrogate for local action potential duration) were computed as the difference between RT and AT. **Supplemental Figure S2** defines these measures. ECGI-reconstructed ARI values were validated against direct intraoperative epicardial mapping in humans (Zhang et al. Online Supplement [16]). Spatial gradient magnitudes of EGM measures were computed for each EGM as the absolute value of the change between neighboring EGMs divided by the distance between EGM locations, averaged across all neighbors. EGM amplitudes were computed as the peak-to-peak voltage during the QRS complex. Fractionation was quantified using the number of steep downward deflections between QRS onset and the start of the T-wave. Additional details of the fractionation quantification and sample EGMs are provided in **Supplemental Figure S3**. The earliest 10% of ATs were considered the epicardial initiation site of a PVC. PVC occurrence rates per EGM at a given epicardial site were computed as the number of times the EGM met the above criterion divided by the total number of beats recorded during the study.

Statistical Analysis

Fractionation values within anatomical segments are presented as z-scores compared to a group of 20 healthy adults. Electrical measures in the ARVC study population were compared to healthy controls using Wilcoxon rank-sum tests. Exercise changes were assessed using Wilcoxon signed-rank tests. Cohort data are presented as medians and quartiles. Substrate and PVC rate

comparisons were performed using Spearman correlation coefficients computed using Matlab software (The MathWorks, Inc., Natick, Massachusetts, USA).

Results

Electrical Substrate at Rest

Abnormal sinus rhythm activation and conduction were common in the ARVC patients. The normal epicardial activation pattern is well described [17] and a representative control is presented in **Figure 1**. Generally, the earliest epicardial activation appears as a breakthrough, most commonly in the anterior RV, and the basal lateral LV is usually the latest region to activate (**Fig 1A**). The normal sinus activation of healthy adult hearts does not have regions of discontinuous conduction or fractionated EGMs (**Fig 1A and 1B, left**). In contrast to the normal activation sequence, we observed abnormal and varied epicardial breakthrough locations, regions of discontinuous conduction, and fractionated electrograms in the ARVC study population.

Figures 2-4 present activation and conduction patterns seen in ARVC patients. In two patients with advanced disease (63 and 66 years old, respectively) we observed earliest epicardial breakthrough in the LV (**Fig 2A** and **3A**). One of these patients had normal epicardial EGMs (**Fig 2A**), while we observed low-amplitude fractionated EGMs in the other (**Fig 3A**). ECGI resolved activation and conduction abnormalities in a 26-year-old patient who did not have any Major Task Force Diagnostic Criteria. In this patient, we observed fractionated EGMs and non-uniform conduction near the earliest epicardial breakthrough site (**Fig 4A**). ARVC patients had

fractionation scores within anatomical regions that ranged from values within the control range (**Fig 2B, top**) to values which were several standard deviations above the control distribution (**Fig 3B and 4B, top**). While some patients had high fractionation scores, we did not observe EGMs in these patients with deflections after the QRS complex (late potentials) that are commonly associated with re-entrant arrhythmias (**Fig 2A-4A**). The abnormal conduction in ARVC patients compared to controls was reflected in statistically longer total duration of epicardial activation ($p = 0.007$, Control: 42 [36-47] ms, ARVC: 52 [44-64] ms) and steeper mean epicardial gradients of AT ($p = 0.018$, Control: 0.24 [0.21-0.28] ms/mm, ARVC: 0.31 [0.26-0.37] ms/mm).

Repolarization in ARVC patients was prolonged compared to controls, and this prolongation was often spatially heterogeneous. **Figure 1B (right)** presents a schematic map of mean ARI values in epicardial segments for a representative control. Control values were homogenous and fell within the range of values previously reported [17]. In contrast, **Figures 2B and 3B (middle)** show prolonged ARI values in ARVC patients. As demonstrated in **Figure 2B (top)**, regions of normal ARI values may co-exist with regions of long ARIs. Mean ventricular ARIs during resting sinus rhythm (Fridericia rate correction applied) were significantly longer than control values ($p = 0.014$, Control: 241 [230-262] ms, ARVC: 275 [238-300] ms). While ARIs were prolonged in ARVC patients, we did not observe increased spatial gradients of repolarization or total duration of epicardial repolarization (**Supplemental Table S4**).

The presence of T-wave inversion on clinical ECG (clinical ECG findings in **Supplemental Table S2**) was strongly associated with ARI prolongation. ARVC patients with T-wave

inversion (Fridericia rate correction applied) had significantly longer mean ARI values than those without inversion ($p = 0.010$, With Inversion: 300 [269-313] ms, Without Inversion: 238 [231-262] ms). However, ECGI identified a patient without T-wave inversion whose mean epicardial ARI was longer than any control, as well as a patient with T-wave inversion whose mean epicardial ARI was within the lowest quartile of the control values (**Supplemental Table S5**).

Electrical Substrate during Stress

As expected, mean epicardial ARI (uncorrected for HR) shortened due to exercise ($p < 0.001$). Total RT ($p = 0.002$), mean epicardial RT gradients ($p = 0.007$), and mean EGM amplitude ($p < 0.001$) also decreased due to exercise. Total AT, mean epicardial AT gradients, and fractionation were unaffected by exercise (**Supplemental Table S6**).

Structural (CMR) Substrate

Advanced LGE revealed a spectrum of scar burden in the ARVC patients. There was scar in 72% of ARVC patients agreeable to contrast. Three patients had isolated RV LGE, seven had isolated LV LGE, three had biventricular LGE, and five had no scar. Six patients in the study cohort had no Task Force CMR defects. Of these six, three had visible LV LGE. **Panels B (bottom) and C of Figures 2-4** illustrate the broad spectrum of LGE observed in the study population.

Relationship of Electrical and Structural Substrates

LGE scar spatially co-localized with EP substrate abnormalities, and the relationship between CMR scar and EP abnormalities was stronger in the LV than in the RV. The amount of LV LGE

within anatomical segments correlated with EGM markers of abnormal depolarization including low amplitude EGMs, increased number of deflections per EGM, and increased AT spatial gradients. LV LGE correlated with prolonged resting ARI values and increase in ARI shortening during and post exercise (**Supplemental Table S7**). RV LGE values within anatomical segments did not correlate with EGM markers of abnormal depolarization, but did correlate with prolonged ARIs at rest and post-exercise. RV LGE correlated with ARI shortening due to exercise (**Supplemental Table S8**).

The results from Patient 6 (**Fig 2**) and Patient 14 (**Fig 3**) illustrate the above findings. Patient 6 has an RV anatomical scar that does not extend to the epicardium, as determined from LGE (**Fig 2C**). The absence of scar on the epicardium is reflected in the local EGMs (**EGM 1, Fig 2A**), which appear normal. This is also reflected in the normal fractionation z-scores (**Fig 2B, top**). Patient 14 has a similar RV anatomical scar, which lacks clear epicardial involvement (**Fig 3C**). However, in this case, the ECGI reconstructed epicardial EGMs at this location (**EGM 1, Fig 3A**) are low amplitude and fractionated, indicating EP abnormality at the epicardium. The same patient also has an LV scar which is visible on the epicardial aspect of the lateral LV. For this scar, the corresponding epicardial EGMs (**EGM 2, Fig 3A**) are fractionated, indicating coexistence of abnormal anatomical and EP substrates on the epicardium.

Ventricular Ectopy

Ventricular ectopy was common in the ARVC patients and occurred more frequently as heart rate increased following exercise. We observed PVCs in fifteen of twenty ARVC patients, with a total of 41 distinct morphologies. The sites of earliest epicardial activation of the PVCs were

spread across both ventricles, with greater involvement of RV and basal locations. A schematic diagram of the earliest epicardial activation sites for all PVC morphologies is provided in **Figure 5**.

The PVC rate within anatomical segments correlated with prolonged ARIs, ARI shortening due to exercise, low voltage EGMs, increased deflections per EGM, and LGE scar (all correlations $p < 0.001$). The PVC rate within anatomical segments did not correlate with increased gradients in AT, RT, or ARI. **Figures 6** and **7** show the temporal occurrence and spatial location and propagation of PVCs in two patients. The substrates for these patients are presented in **Figures 2** and **3**, respectively. **Supplemental Table S9** summarizes the correlations between PVC rate and structural and EP substrate measures.

Discussion

This is the first evaluation of ECGI in ARVC patients. ECGI was sensitive enough to detect EP substrate differences between ARVC patients and healthy controls. By combining ECGI with LGE, we determined correlations between EP abnormalities and LGE scar. These correlations indicate that the EP abnormalities detected with ECGI are markers of disease progression. Importantly, new findings regarding properties of the EP and scar substrates included prolonged epicardial ARIs and a relationship of PVC rate within a region to repolarization, EP markers of scar, and LGE.

ARVC Scar Substrate

Ventricular LGE was variable in location and extent. LV LGE was a more frequent finding than RV LGE. LV LGE co-localized with traditional markers of EP scar assessed using ECGI, as reflected by its correlation with lower voltage EGMs and increased fractionation. This finding mirrors prior ECGI studies that found regions of scar assessed with LGE or single-photon emission computed tomography to have lower voltage EGMs and increased fractionation [18]. In the RV, we did not observe a strong relationship between LGE and traditional EP markers of scar. This is consistent with prior work comparing invasive EP mapping to RV LGE, which found that nearly 50% of electrical scar substrates in the RV were not confirmed by LGE [19]. Prior studies have suggested that the absence of RV LGE findings could be attributed to the thin RV wall, which complicates LGE in the RV [20]. Alternatively, it is possible that EP abnormalities in the RV manifest in the presence of minimal scar or scar that is diffuse and not easily resolved with current imaging techniques.

Prolongation of Repolarization

There are multiple mechanisms which could contribute to the ARI prolongation observed in this study. Functional changes in ionic currents due to ARVC mutations could contribute to prolonged repolarization. Studies linking I_{Na} current to Plakophilin-2 mutations provided the first evidence that ARVC may have some features of a channelopathy [21]. While the focus of research efforts in this area has largely been on depolarization, it is possible that repolarizing currents are altered as well. $K_v1.5$ channels localize to the intercalated disc and associate with $Na_v1.5$ [22,23], and $K_v1.5$ function depends on N-cadherin, an intercalated disc protein [24]. A mutation in KCNE2 that inhibits trafficking of $K_v1.5$ to the intercalated disc causes prolonged repolarization [25]. While

we are unaware of direct evidence suggesting that this mechanism is involved in ARVC, it is an interesting avenue for exploration.

Another mechanism which may contribute to prolonged repolarization is progression of the heart failure phenotype associated with ARVC. Heart failure is a known end-stage complication of ARVC [4], but systolic impairment of varying degrees can appear in either or both ventricles in the absence of clinical heart failure [10]. Action potential prolongation is a hallmark of heart failure along with functional downregulation of potassium currents, slow conduction, and abnormal calcium homeostasis [26]. It is possible that these features develop in ARVC patients either globally or locally as the disease progresses and surviving myocardium is subjected to increasing strains because of fibrofatty tissue replacement.

Finally, myocardial uncoupling can increase the effects of any action potential duration prolongation mechanisms. Myocardial uncoupling facilitates gradients in repolarization by decreasing the electrotonic coupling between cells [27]. Fibrofatty replacement acts to uncouple cells by decreasing the local density of excitable cells. Reduction in the number and size of gap junctions in the intercalated disc causes further uncoupling in ARVC, and has been reported even in histologically normal regions of myocardium [6].

In our data, ARI prolongation correlated with LGE in both ventricles. This suggests that the uncoupling effect of the scar, altered mechanical strains in regions of scar, or both may be important to the development of prolonged repolarization. The uncoupling effect of ventricular scar could also contribute to the correlation we observed between stress-related ARI shortening

and LGE in both ventricles, as both rate increase and sympathetic stimulation have a greater effect on cardiomyocytes that are less electrically coupled. While our population size is not sufficient to draw conclusions about the age progression of the ARVC phenotype, we note that the group included two patients in their twenties, both of whom had ARI values within the normal range. This suggests that action potential prolongation in ARVC patients may develop as the overall phenotype progresses. Mean epicardial ARIs were generally longer in patients with precordial lead T-wave inversion. However, there were patients with and without T-wave inversion who were exceptions to this relationship, indicating that ECGI offers improved sensitivity and specificity for detecting prolonged repolarization. Additionally, ECGI provides spatial information about ARI prolongation, which was spatially heterogeneous in ARVC.

Arrhythmia Triggers (PVCs)

The ability of ECGI to panoramically map the whole heart in a single beat allowed us to localize PVCs, determine the frequency of each unique PVC morphology, and correlate ectopic frequency with the EP and scar substrates. The overall rate of PVCs was increased by exercise. We found that PVC rate within anatomical segments correlated with local ARI prolongation, increased ARI shortening due to exercise, low voltage EGMs, fractionated EGMs, and LGE.

The hallmark finding of progressive scar formation in ARVC is compatible with the possibility of re-entrant circuit formation. Prior work demonstrated conduction slowing at elevated heart rates in ARVC patients [28]. In the present study, we found evidence of slow conduction in the form of longer total activation times and steeper activation gradients relative to controls. However, we did not observe the dynamic conduction slowing at elevated HRs that Finlay et al.

reported [28]. This discrepancy could be attributable to the difference in HRs investigated. In the present study, patients exercised to a peak HR of 120 beats/min, whereas the patients in the Finlay et al. study were paced at an interval just below the ventricular refractory period.

The combination of scar, slow conduction, and prolonged repolarization could facilitate unidirectional block and reentrant arrhythmia. Important signatures of re-entrant arrhythmia are EGM fractionation and late potentials. We did not observe late potentials in the reconstructed EGMs. This stands in contrast to ECGI studies of post-infarction scar-related ventricular tachycardia, which found a high prevalence of late potentials with re-entry circuits closely related to the EP substrate [29]. While this could indicate that re-entrant arrhythmias are less prevalent in ARVC, it is important to note the significant differences in the anatomy of the scars in each population. Post–infarction scars are often large and heterogeneous, with large islands of surviving myocardium, especially in the border zone. The ARVC scar substrate, on the other hand, accumulates gradually over time and is typically diffuse, originating from the epicardium. It is possible that the lower regional density of surviving myocardium in ARVC scar makes it difficult to resolve late potentials in EP mapping of ARVC patients.

Focal mechanisms may cause arrhythmia triggers in ARVC patients. Focal triggered activity is commonly observed in isolated myocytes in the form of early afterdepolarizations or delayed afterdepolarizations. Early afterdepolarizatons at plateau potentials are caused by recovery and re-activation of I_{Ca}, with the delayed rectifier currents, I_{Kr} and I_{Ks}, playing an important role [30]. We observed that PVC rate correlated with regions of prolonged ARI, a surrogate for local action potential duration, including during stress when I_{Ca} is augmented by beta-adrenergic stimulation.

Action potential duration prolongation increases the window for I_{Ca} re-activation and early afterdepolarization formation. In the intact heart, electrotonic coupling between myocytes acts as a current sink for depolarizing currents. Reduced coupling, caused by scar and gap junction abnormalities in ARVC, can increase the likelihood of focal activity by decreasing the current sink effect. The observed correlation between PVC rate and electrical and LGE markers of scar suggests that an uncoupling effect is present at PVC initiation sites. It is interesting to note that Myles et al. [31] found that focal activity was more common in the RV, which they attributed to reduced coupling in the thin RV wall compared to the LV. In our study, we found greater overall ectopy in the RV.

Clinical Implications

The progressive nature of ARVC and its early concealed phase complicate diagnosis and treatment. CMR currently plays a valuable role in the evaluation of ventricular structure and function. The current Task Force criteria do not include LGE, but acknowledge that it may be included in future revisions [3]. Our data show that combined ECGI and LGE could increase the sensitivity for detecting substrate abnormalities in ARVC patients, including young patients with little or no Task Force MRI and ECG criteria. LGE and ECGI are compatible with the current use of CMR in the diagnosis and longitudinal assessment of ARVC. These imaging techniques can be performed in addition to the conventional CMR assessment to provide a thorough characterization of structural, functional, and EP abnormalities. In the present study, we report a spectrum of abnormalities using these techniques and demonstrate a relationship between the

imaged substrates and ventricular ectopy. Since ventricular ectopy may play a causal role in triggering arrhythmias, combined ECGI and LGE may have a role in risk stratification.

Limitations

This study is a first evaluation of combined ECGI and LGE in ARVC patients and, therefore, evaluated a relatively small group of twenty patients. Because CMR is commonly contraindicated in patients with implanted devices, we only recruited patients without ICDs. While this choice enabled us to image LGE in the study cohort, a drawback is that none of the patients in this study had prior episodes of ventricular tachycardia. Therefore, this study cohort is not well-suited for evaluating sudden cardiac death risk stratification. Further studies are necessary to explore this application of these techniques. The current study evaluated patients ranging in age from 24 to 75 years old; however, only three patients were younger than 41 years old. Future studies should evaluate whether this approach can detect the presence of ARVC in young, asymptomatic and genotype-positive individuals. Larger studies of a wide range of ages and genotypes are important for exploring the progression of the disease, including how the EP and scar substrates change over time. Prior studies demonstrated that strain imaging may be effective for detecting the early stages of ARVC and for risk stratification [32,33]. Future studies could combine ECGI and strain imaging into a multi-modality approach for ARVC diagnosis and risk stratification. Exercise and LGE data were collected from the ARVC patients, but not controls. These data are needed to establish ranges for healthy controls. Additional data are necessary to determine the specificity of ECGI and LGE criteria for diagnosis of ARVC.

Conclusion

ECGI in combination with advanced LGE reveals a spectrum of electrical and structural substrate abnormalities in ARVC patients. This combination may improve sensitivity for detecting ARVC substrate abnormalities. These data suggest a role for combined ECGI and LGE in early diagnosis, non-invasive follow-up, and risk stratification of ARVC patients.

Funding Sources

This study was supported by NIH – National Heart, Lung and Blood Institute grants R01-HL-033343 and R01-HL-049054 (to YR) and by Washington University Institute of Clinical and Translational Sciences grant UL1-TR000448 from the National Center for Advancing Translational Sciences of the NIH. The Royal Academy of Engineering provided support for YR while in the UK, under the Distinguished Visiting Fellowships-Round 5 scheme. Dr. Rudy is the Fred Saigh Distinguished Professor at Washington University. The University College London Hospitals Biomedicine NIHR & Barts Charity provided additional support for this work. NTS was supported by a British Heart Foundation Clinical Research Training Fellowship (FS/14/9/30407). MO was supported by a Marie Curie Fellowship (IEF-2013). PL and PT were supported by the Medical Research Council (G0901819).

Disclosures

YR receives royalties from CardioInsight Technologies (CIT). CIT does not support any research conducted in Dr. Rudy's laboratory.

References

1. Sen-Chowdhry S, Morgan RD, Chambers JC, McKenna WJ. Arrhythmogenic cardiomyopathy: etiology, diagnosis, and treatment. *Annu Rev Med*. 2010;61:233–253.

2. Asimaki A, Kleber AG, Saffitz JE. Pathogenesis of Arrhythmogenic Cardiomyopathy. *Can J Cardiol*. 2015;31:1313–1324.

3. Marcus FI, McKenna WJ, Sherrill D, Basso C, Bauce B, Bluemke DA, Calkins H, Corrado D, Cox MGPJ, Daubert JP, Fontaine G, Gear K, Hauer R, Nava A, Picard MH, Protonotarios N, Saffitz JE, Sanborn DMY, Steinberg JS, Tandri H, Thiene G, Towbin JA, Tsatsopoulou A, Wichter T, Zareba W. Diagnosis of Arrhythmogenic Right Ventricular Cardiomyopathy/Dysplasia: Proposed Modification of the Task Force Criteria. *Circulation*. 2010;121:1533–1541.

4. Corrado D, Wichter T, Link MS, Hauer RNW, Marchlinski FE, Anastasakis A, Bauce B, Basso C, Brunckhorst C, Tsatsopoulou A, Tandri H, Paul M, Schmied C, Pelliccia A, Duru F, Protonotarios N, Estes NM, McKenna WJ, Thiene G, Marcus FI, Calkins H. Treatment of Arrhythmogenic Right Ventricular Cardiomyopathy/Dysplasia: An International Task Force Consensus Statement. American Heart Association Journals; 2015. p. 441–453.

5. Basso C, Thiene G, Corrado D, Angelini A, Nava A, Valente M. Arrhythmogenic right ventricular cardiomyopathy. Dysplasia, dystrophy, or myocarditis? *Circulation*. 1996;94:983–991.

6. Delmar M, McKenna WJ. The cardiac desmosome and arrhythmogenic cardiomyopathies: from gene to disease. *Circ Res*. 2010;107:700–714.

7. Cerrone M, Delmar M. Desmosomes and the sodium channel complex: implications for arrhythmogenic cardiomyopathy and Brugada syndrome. *Trends Cardiovasc Med*. 2014;24:184–190.

8. Rojas A, Calkins H. Present understanding of the relationship between exercise and arrhythmogenic right ventricular dysplasia/cardiomyopathy. *Trends Cardiovasc Med*. 2015;25:181–188.

9. Gomes J, Finlay M, Ahmed AK, Ciaccio EJ, Asimaki A, Saffitz JE, Quarta G, Nobles M, Syrris P, Chaubey S, McKenna WJ, Tinker A, Lambiase PD. Electrophysiological abnormalities precede overt structural changes in arrhythmogenic right ventricular cardiomyopathy due to mutations in desmoplakin-A combined murine and human study. *European heart journal*. 2012;33:1942–1953.

10. Sen-Chowdhry S, Syrris P, Ward D, Asimaki A, Sevdalis E, McKenna WJ. Clinical and genetic characterization of families with arrhythmogenic right ventricular dysplasia/cardiomyopathy provides novel insights into patterns of disease expression. *Circulation*. 2007;115:1710–1720.

11. Zorzi A, Rigato I, Bauce B, Pilichou K, Basso C, Thiene G, Iliceto S, Corrado D. Arrhythmogenic Right Ventricular Cardiomyopathy: Risk Stratification and Indications for Defibrillator Therapy. *Curr Cardiol Rep*. 2016;18:57–11.

12. Marchlinski FE, Edvardsen T. Arrhythmogenic Right Ventricular Cardiomyopathy: Better Tools for Detecting Early Disease and Progression. *J Am Coll Cardiol*. 2016;68:2198–2200.

13. Ramanathan C, Ghanem RN, Jia P, Ryu K, Rudy Y. Noninvasive electrocardiographic imaging for cardiac electrophysiology and arrhythmia. *Nat Med*. 2004;10:422–428.

14. Kellman P, Arai AE. Cardiac imaging techniques for physicians: late enhancement. *J Magn Reson Imaging*. 2012;36:529–542.

15. Coronel R, Debakker J, Wilmsschopman F, Opthof T, Linnenbank A, Belterman C, Janse M. Monophasic action potentials and activation recovery intervals as measures of ventricular action potential duration: Experimental evidence to resolve some controversies. *Heart Rhythm*. 2006;3:1043–1050.

16. Zhang J, Hocini M, Strom M, Cuculich PS, Cooper DH, Sacher F, Orini M, Lambiase PD, Taggart P, Haïssaguerre M, Rudy Y (With contribution to Section 1 of Online Supplement by Orini M, Lambiase PD, Taggart P). The Electrophysiological Substrate of Early Repolarization Syndrome: Noninvasive Mapping in Patients. *J Am Coll Cardiol EP*. In Press.

17. Ramanathan C, Jia P, Ghanem R, Ryu K, Rudy Y. Activation and repolarization of the normal human heart under complete physiological conditions. *Proc Natl Acad Sci USA*. 2006;103:6309–6314.

18. Cuculich PS, Zhang J, Wang Y, Desouza KA, Vijayakumar R, Woodard PK, Rudy Y. The electrophysiological cardiac ventricular substrate in patients after myocardial infarction: noninvasive characterization with electrocardiographic imaging. *J Am Coll Cardiol*. 2011;58:1893–1902.

19. Marra MP, Leoni L, Bauce B, Corbetti F, Zorzi A, Migliore F, Silvano M, Rigato I, Tona F, Tarantini G, Cacciavillani L, Basso C, Buja G, Thiene G, Iliceto S, Corrado D. Imaging study of ventricular scar in arrhythmogenic right ventricular cardiomyopathy: comparison of 3D standard electroanatomical voltage mapping and contrast-enhanced cardiac magnetic resonance. *Circulation Arrhythmia and electrophysiology*. 2012;5:91–100.

20. Riele Te ASJM, Tandri H, Bluemke DA. Arrhythmogenic right ventricular cardiomyopathy (ARVC): cardiovascular magnetic resonance update. *J Cardiovasc Magn Reson*. 2014;16:50.

21. Sato PY, Musa H, Coombs W, Guerrero-Serna G, Patiño GA, Taffet SM, Isom LL, Delmar M. Loss of plakophilin-2 expression leads to decreased sodium current and slower conduction velocity in cultured cardiac myocytes. *Circ Res*. 2009;105:523–526.

22. Mays DJ, Foose JM, Philipson LH, Tamkun MM. Localization of the Kv1.5 K+ channel protein in explanted cardiac tissue. *J Clin Invest*. 1995;96:282–292.

23. Milstein ML, Musa H, Balbuena DP, Anumonwo JMB, Auerbach DS, Furspan PB, Hou L, Hu B, Schumacher SM, Vaidyanathan R, Martens JR, Jalife J. Dynamic reciprocity of sodium and potassium channel expression in a macromolecular complex controls cardiac excitability and arrhythmia. *Proc Natl Acad Sci USA*. 2012;109:E2134–43.

24. Cheng L, Yung A, Covarrubias M, Radice GL. Cortactin is required for N-cadherin regulation of Kv1.5 channel function. *J Biol Chem*. 2011;286:20478–20489.

25. Roepke TK, Kontogeorgis A, Ovanez C, Xu X, Young JB, Purtell K, Goldstein PA, Christini DJ, Peters NS, Akar FG, Gutstein DE, Lerner DJ, Abbott GW. Targeted deletion of kcne2 impairs ventricular repolarization via disruption of I(K,slow1) and I(to,f). *FASEB J*. 2008;22:3648–3660.

26. Aiba T, Tomaselli GF. Electrical remodeling in the failing heart. *Curr Opin Cardiol*. 2010;25:29–36.

27. Viswanathan PC, Shaw RM, Rudy Y. Effects of IKr and IKs heterogeneity on action potential duration and its rate dependence: a simulation study. *Circulation*. 1999;99:2466–2474.

28. Finlay MC, Ahmed AK, Sugrue A, Bhar-Amato J, Quarta G, Pantazis A, Ciaccio EJ, Syrris P, Sen-Chowdhry S, Ben-Simon R, Chow AW, Lowe MD, Segal OR, McKenna WJ, Lambiase PD. Dynamic conduction and repolarisation changes in early arrhythmogenic right ventricular cardiomyopathy versus benign outflow tract ectopy demonstrated by high density mapping & paced surface ECG analysis. *PLoS ONE*. 2014;9:e99125.

29. Zhang J, Cooper DH, Desouza KA, Cuculich PS, Woodard PK, Smith TW, Rudy Y. Electrophysiologic Scar Substrate in Relation to VT: Noninvasive High-Resolution Mapping and Risk Assessment with ECGI. *Pacing Clin Electrophysiol*. 2016;39:781–791.

30. Zeng J, Rudy Y. Early afterdepolarizations in cardiac myocytes: mechanism and rate dependence. *BPJ*. 1995;68:949–964.

31. Myles RC, Wang L, Kang C, Bers DM, Ripplinger CM. Local β-adrenergic stimulation overcomes source-sink mismatch to generate focal arrhythmia. *Circ Res*. 2012;110:1454–1464.

32. Mast TP, Teske AJ, Walmsley J, Van Der Heijden JF, van Es R, Prinzen FW, Delhaas T, van Veen TA, Loh P, Doevendans PA, Cramer MJ, Lumens J. Right Ventricular Imaging and Computer Simulation for Electromechanical Substrate Characterization in Arrhythmogenic Right Ventricular Cardiomyopathy. *J Am Coll Cardiol*. 2016;68:2185–2197.

33. Sarvari SI, Haugaa KH, Anfinsen OG, Leren TP, Smiseth OA, Kongsgaard E, Amlie JP, Edvardsen T. Right ventricular mechanical dispersion is related to malignant arrhythmias: a study of patients with arrhythmogenic right ventricular cardiomyopathy and subclinical right ventricular dysfunction. *European heart journal*. 2011;32:1089–1096.

Tables

Table 1

Patient ID	Age	Gender	Mutation	Major Criteria	Minor Criteria
1	59	M	JUP	1	1
2	63	M	PKP2	1	3
3	54	F	PKP2	2	3
4	44	M	DSP	1	3
5	55	M	DSP	1	5
6	63	M	PKP2	3	3
7	59	M	DSP	1	3
8	69	F	PKP2	0	2
9	61	M	DSP	1	2
10	41	F	DSP*	1	1
11	49	F	PKP2	3	2
12	60	M	DSG	3	2
13	26	M	PKP2	0	3
14	66	M	PKP2	2	1
15	54	M	PKP2	2	0
16	74	M	DSG	1	3
17	24	M	DSP	1	0
18	54	M	Negative	2	2
19	39	M	Negative	2	2
20	75	M	Negative	2	3

ARVC patient characteristics including Task Force Major and Minor Criteria (numbers indicate how many Major and Minor Criteria were observed). Mutation abbreviations: Plakoglobin (JUP), Plakophilin-2 (PKP2), Desmoplakin (DSP), Desmoglein (DSG). Asterisk indicates variant of unknown significance.

Figure Legends

Figure 1

Electrical substrate in a healthy adult. (**A**) Sinus rhythm activation with a typical RV epicardial breakthrough (asterisk) and normal conduction. RV (1) and LV (2) unipolar EGMs have a normal morphology free of fractionation. (**B**) Schematic maps of normal electrical properties in anatomical regions based on 20 control subjects. Left: fractionation z-score. Right: Fridericia-corrected ARI. The maps show absence of fractionation and ARI values within the normal range. AT: activation time. RA: right atrium. LA: left atrium. RV: right ventricle. LV: left ventricle. ARI: activation-recovery interval. EGM: electrogram.

Figure 2

Electrical substrate of a patient (Patient 6) with advanced disease and a high PVC rate (18.69%). (**A**) Ventricular epicardial breakthrough during sinus rhythm was abnormal, with earliest activation originating from the basal inferior LV (asterisk). RV (1) and LV (2) unipolar EGMs had normal QRS morphology. (**B**) EGM fractionation was not abnormal compared to controls (top). Fridericia-corrected ARIs were prolonged compared to control values (middle). Concentrated LGE was visible in the inferior RV (bottom). (**C**) MRI image of extensive LGE, which was confined to the subepicardial RV (indicated by yellow arrows). PVC: premature ventricular contraction.

Figure 3

Electrical substrate of a patient (Patient 14) with biventricular disease and a moderate PVC rate (1.11%). (**A**) Sinus rhythm breakthrough was abnormal, with earliest epicardial activation originating from the basal lateral LV (asterisk). RV (1) and LV (2) unipolar EGMs were fractionated (note the voltage scale of low-amplitude EGM 1). (**B**) Regions of high fractionation were present in both ventricles (top), and Fridericia-corrected ARI values were prolonged compared to control values (middle). LGE was visible in both ventricles (bottom). (**C**) MRI image of LGE showing scar in both ventricles (yellow arrows).

Figure 4

Electrical substrate of a 26-year-old male (Patient 13) with early disease and no observed PVCs. (**A**) Sinus rhythm epicardial breakthrough occurred in the inferolateral RV (asterisk in inset) with early activation of the RV free wall. There was a region of non-uniform conduction and fractionated unipolar EGMs (1) between these sites. Remote LV unipolar EGM (2) had a normal morphology. (**B**) Fractionation in the RV was much greater than control values (top) while Fridericia-corrected ARI values were within the normal range of controls (middle). Minimal LGE was visible in the LV (bottom). (**C**) MRI showed minimal abnormalities (arrow).

Figure 5

Schematic diagram of earliest epicardial activation of all observed PVC morphologies. Each marker represents a unique PVC morphology, with the number indicating the number of times the morphology was observed during the study. Marker color and shape identify patient ID (indicated below diagram). Sites near the epicardial aspect of the septum are shown on the edge of the RV.

Figure 6

PVC onset and initiation sites of a patient (Patient 6) with a high PVC burden (18.69%). (A) Time-course of observed PVCs in relation to exercise and schematic map of PVC initiation sites. The different PVC initiation sites are labeled A, B, and C and color coded. PVCs occurred only after the onset of exercise, and morphology C appeared only once near peak HR (B) Activation isochrone maps of the three distinct PVC morphologies observed in this patient. Asterisks indicate PVC initiation sites. Morphology B showed very a broad region of early epicardial activation, indicating a possible sub-epicardial origin and possible conduction system involvement. HR: heart rate.

Figure 7

PVC onset and initiation sites of a patient (Patient 14) with a moderate PVC burden (1.11%). (A) Time-course of observed PVCs in relation to exercise and schematic map of PVC initiation sites. Note that morphology C is partially obscured in the post-exercise recording period. (B) Activation isochrone maps of the three distinct PVC morphologies observed in this patient. Asterisks indicate PVC initiation sites.

Figure 1

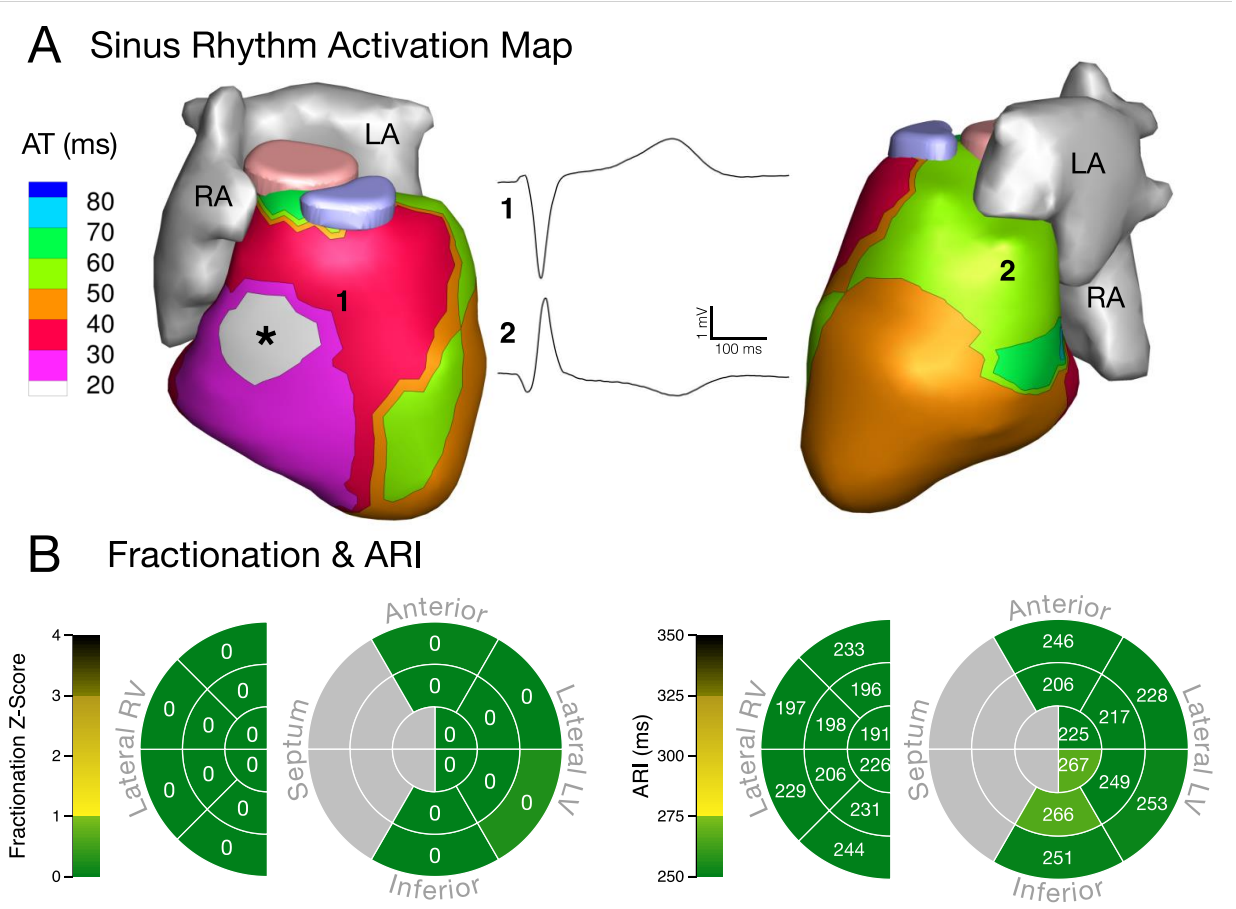
A Sinus Rhythm Activation Map
AT (ms)
80
70
60
50
40
30
20
LA
RA
1
*
2
1 mV
100 ms
LA
RA
2
B Fractionation & ARI
Fractionation Z-Score
4
3
2
1
0
Lateral RV
Anterior
Septum
Lateral LV
Inferior
ARI (ms)
350
325
300
275
250
233
196
197
198
191
226
206
229
231
244
246
206
228
217
225
267
249
253
266
251

Figure 2

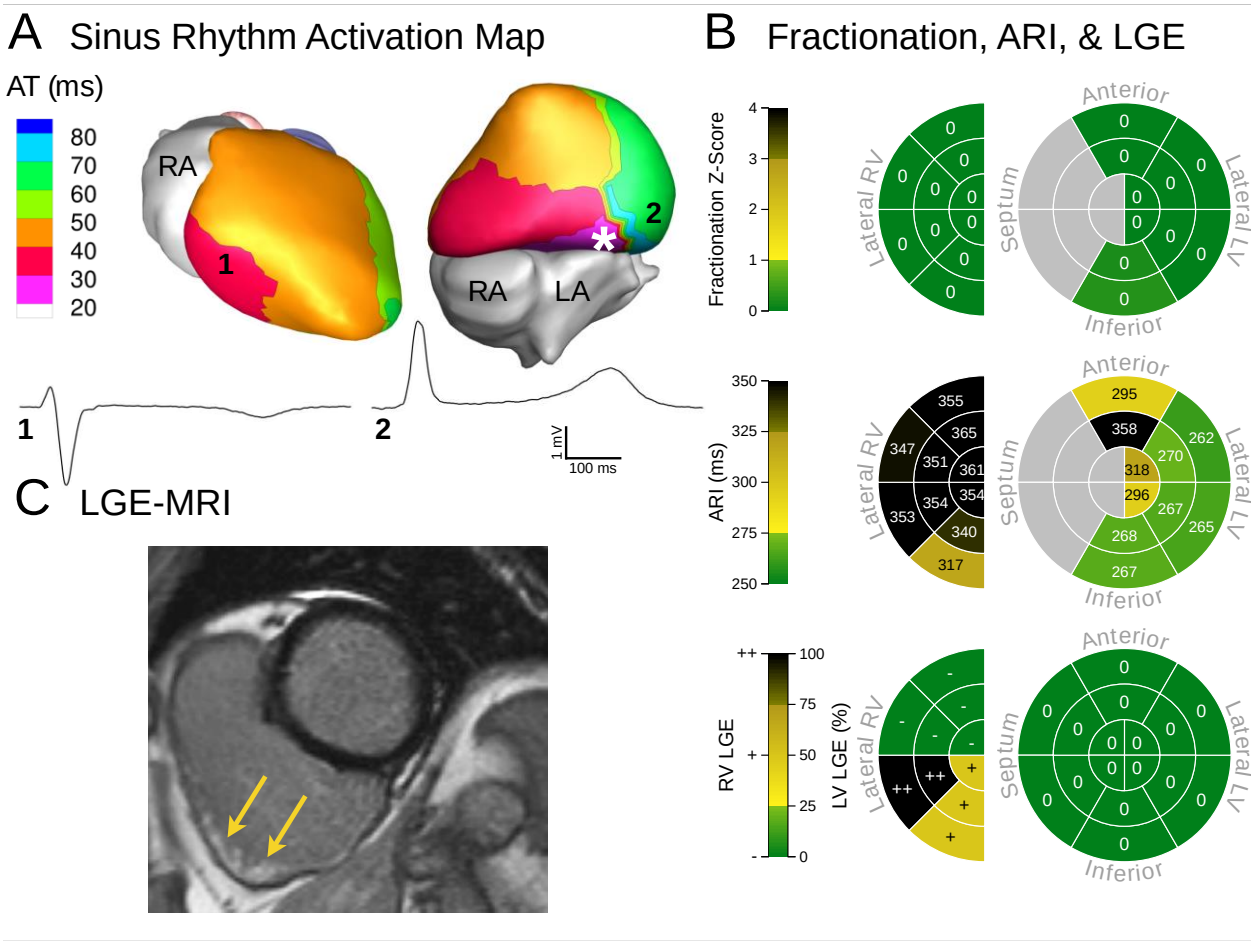
A Sinus Rhythm Activation Map
AT (ms)
80
70
60
50
40
30
20
RA
1
2
RA
LA
1
2
1 mV
100 ms
C LGE-MRI
B Fractionation, ARI, & LGE
Fractionation Z-Score
4
3
2
1
0
ARI (ms)
350
325
300
275
250
RV LGE
++
+
-
LV LGE (%)
100
75
50
25
0
Lateral RV
Anterior
Septum
Lateral LV
Inferior
355
365
347
351
361
354
353
354
340
317
295
358
262
270
318
296
267
265
268
267

Figure 3

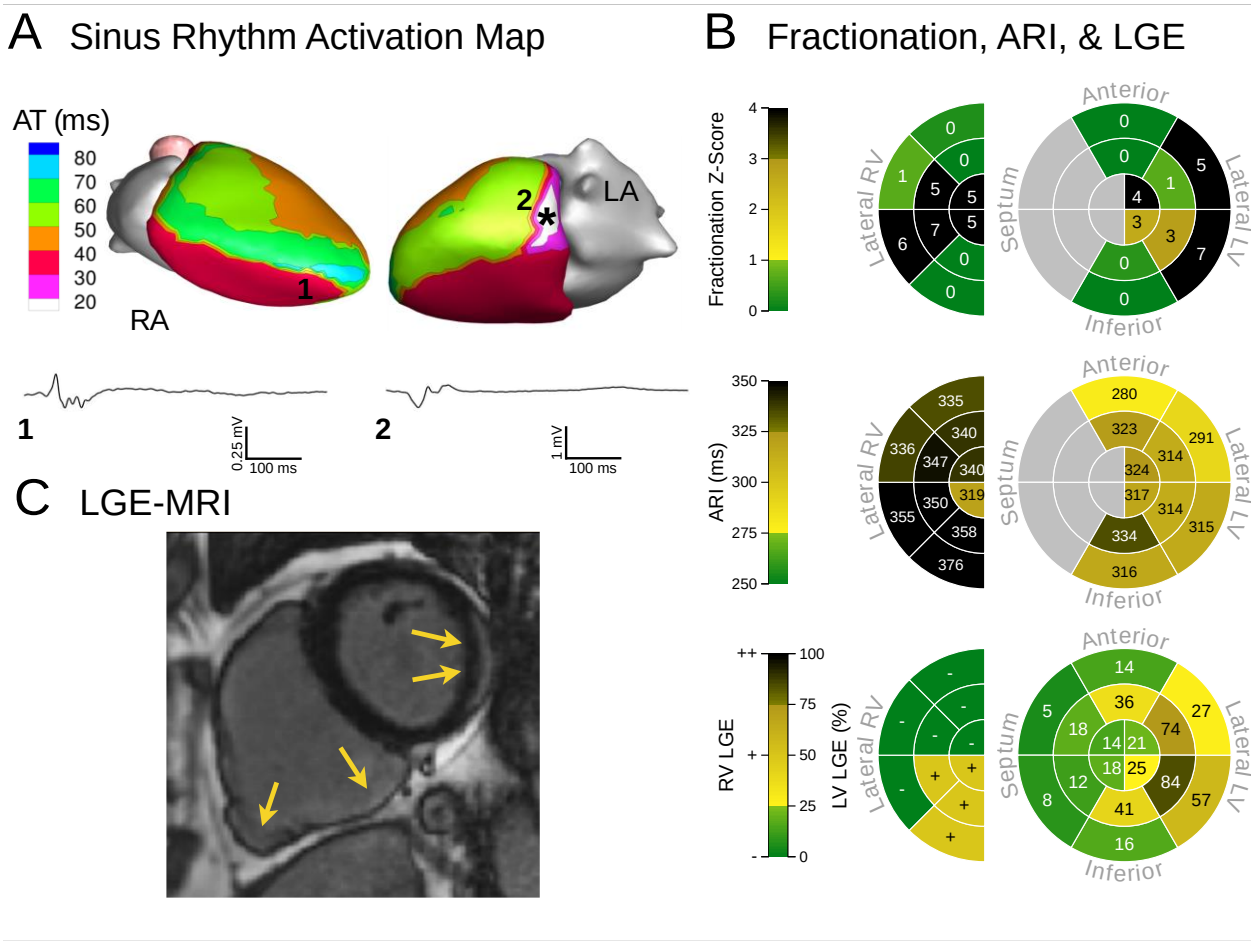
A Sinus Rhythm Activation Map
AT (ms)
80
70
60
50
40
30
20
RA
LA
1
2
*
0.25 mV
100 ms
1 mV
100 ms
C LGE-MRI
B Fractionation, ARI, & LGE
Fractionation Z-Score
4
3
2
1
0
ARI (ms)
350
325
300
275
250
RV LGE
++
+
-
LV LGE (%)
100
75
50
25
0
Anterior
Septum
Lateral LV
Lateral RV
Inferior

Figure 4

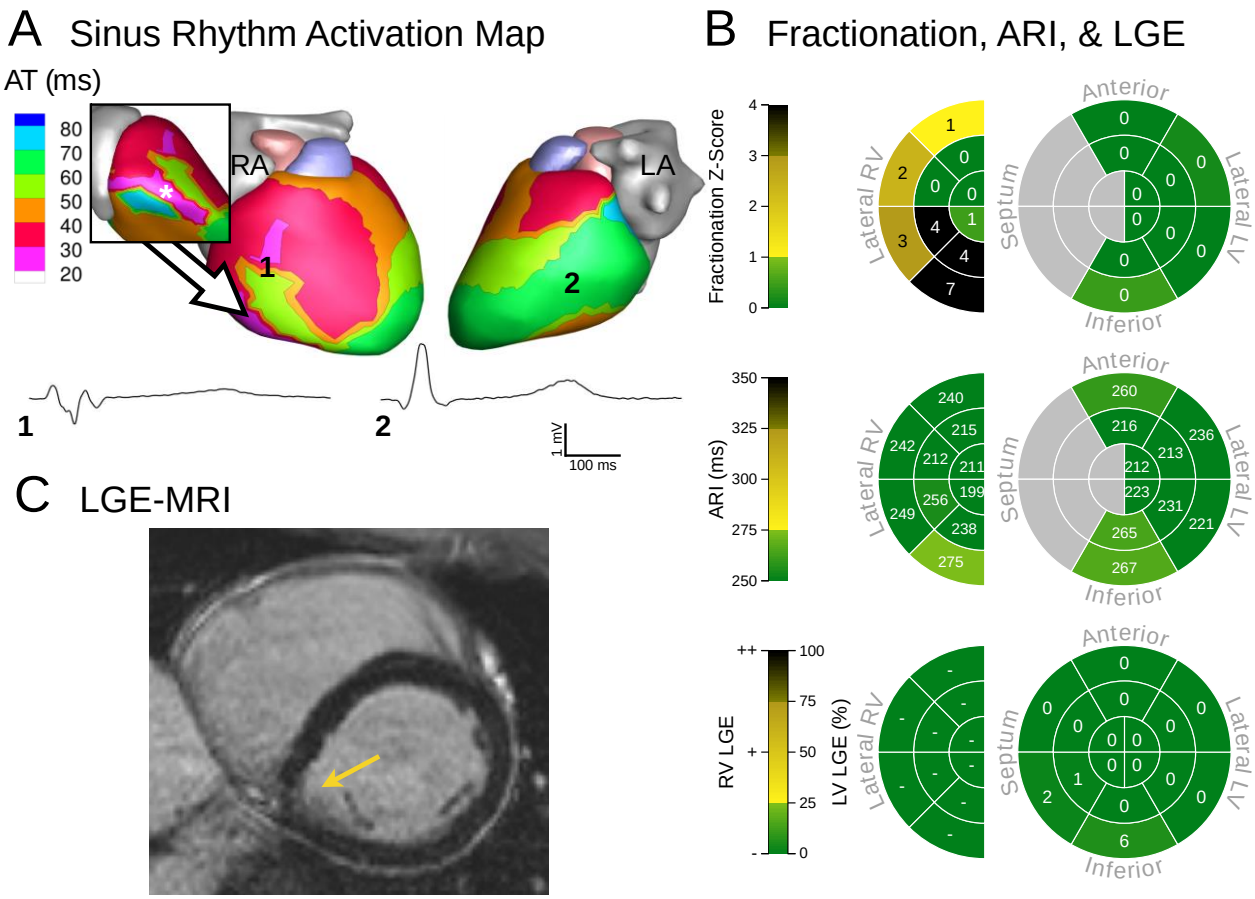
A Sinus Rhythm Activation Map
AT (ms)
80
70
60
50
40
30
20
RA
LA
1
2
1
2
1 mV
100 ms
B Fractionation, ARI, & LGE
Fractionation Z-Score
4
3
2
1
0
ARI (ms)
350
325
300
275
250
RV LGE
++
+
-
LV LGE (%)
100
75
50
25
0
Lateral RV
Septum
Anterior
Lateral LV
Inferior
C LGE-MRI

Figure 5

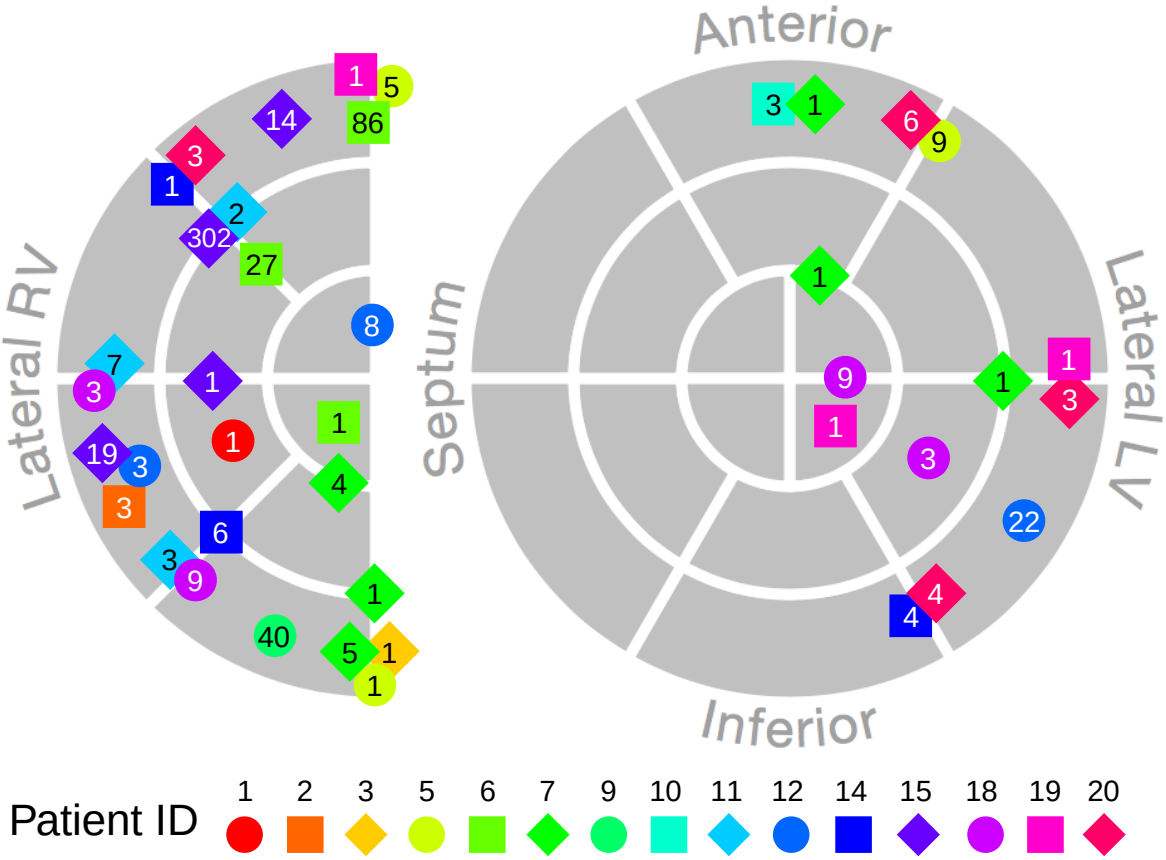
Anterior
Lateral RV
Septum
Lateral LV
Inferior
Patient ID
1 2 3 5 6 7 9 10 11 12 14 15 18 19 20

Figure 6

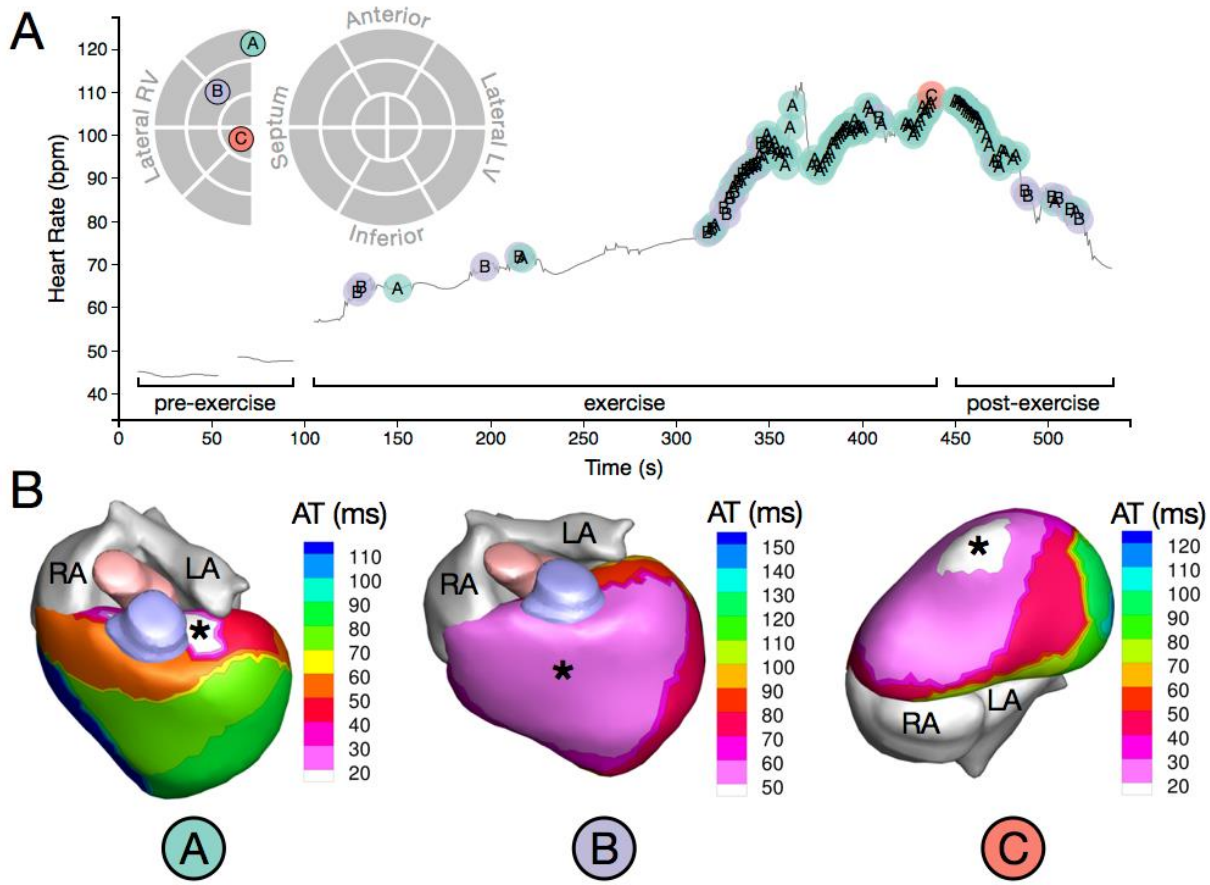
A
Anterior
Lateral RV
Septum
Lateral LV
Inferior
A
B
C
Heart Rate (bpm)
120
110
100
90
80
70
60
50
40
pre-exercise
exercise
post-exercise
0
50
100
150
200
250
300
350
400
450
500
Time (s)
B
RA
LA
AT (ms)
110
100
90
80
70
60
50
40
30
20
150
140
130
120
110
100
90
80
70
60
50
120
110
100
90
80
70
60
50
40
30
20
A
B
C

Figure 7

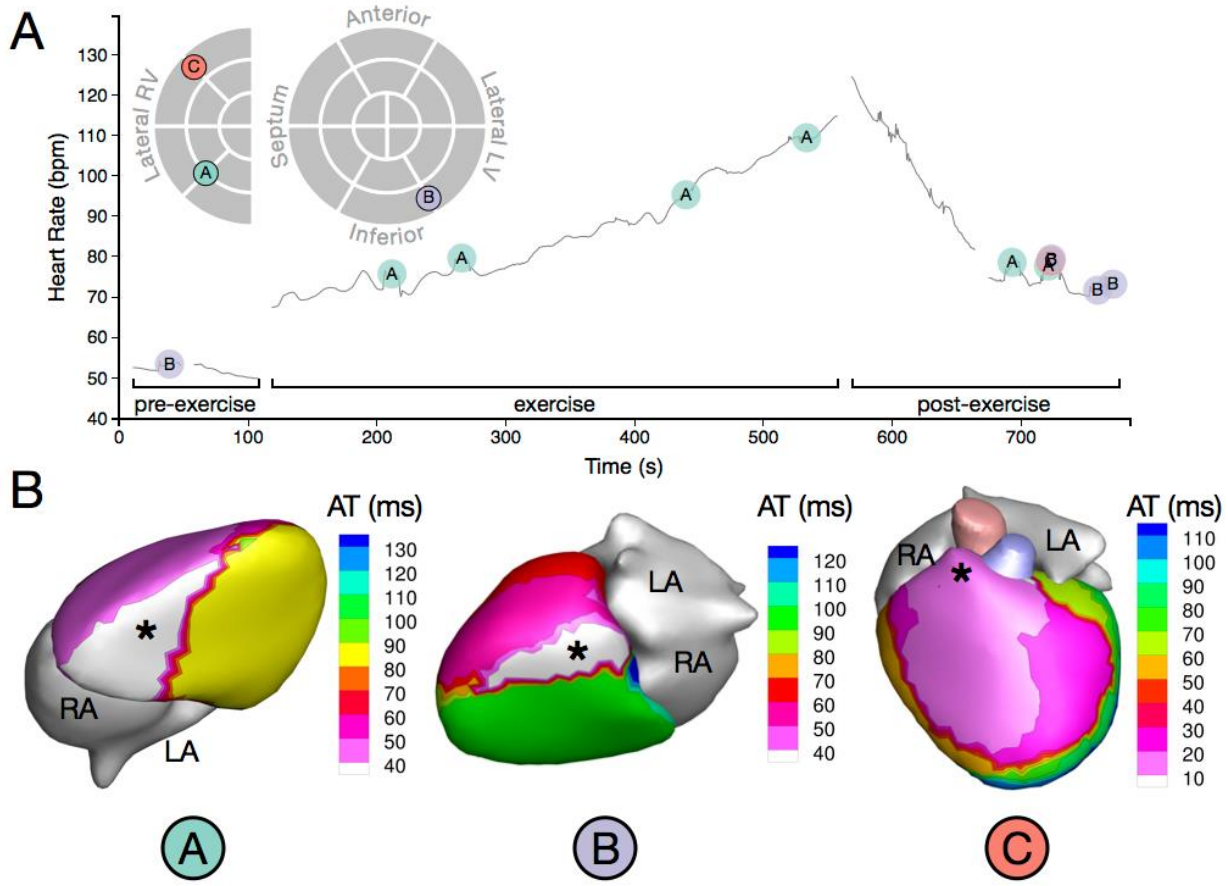
A
Anterior
Lateral RV
Septum
Lateral LV
Inferior
Heart Rate (bpm)
130
120
110
100
90
80
70
60
50
40
0
100
200
300
400
500
600
700
Time (s)
pre-exercise
exercise
post-exercise
B
AT (ms)
130
120
110
100
90
80
70
60
50
40
RA
LA
AT (ms)
120
110
100
90
80
70
60
50
40
LA
RA
AT (ms)
110
100
90
80
70
60
50
40
30
20
10
RA
LA
A
B
C